





Almost global convergence to practical synchronization in the generalized Kuramoto model on networks over the n -sphere

Johan Markdahl ¹, Daniele Proverbio ¹, La Mi¹ & Jorge Goncalves ^{1,2}

From the flashing of fireflies to autonomous robot swarms, synchronization phenomena are ubiquitous in nature and technology. They are commonly described by the Kuramoto model that, in this paper, we generalise to networks over n -dimensional spheres. We show that, for almost all initial conditions, the sphere model converges to a set with small diameter if the model parameters satisfy a given bound. Moreover, for even n , a special case of the generalized model can achieve phase synchronization with nonidentical frequency parameters. These results contrast with the standard $n = 1$ Kuramoto model, which is multistable (i.e., has multiple equilibria), and converges to phase synchronization only if the frequency parameters are identical. Hence, this paper shows that the generalized network Kuramoto models for $n \geq 2$ displays more coherent and predictable behavior than the standard $n = 1$ model, a desirable property both in flocks of animals and for robot control.

¹Luxembourg Centre for Systems Biomedicine, University of Luxembourg, Belvaux, Luxembourg. ²Department of Plant Sciences, University of Cambridge, Cambridge, United Kingdom. ✉email: markdahl@kth.se

Starting with Winfree's seminal work in the late 1960s¹, synchronization phenomena have attracted the interests of scientists in physics and other disciplines^{2–4} and still remain an active area of research with many open problems. One of the most successful descriptors of synchronization phenomena is the Kuramoto model, along with its many generalizations^{3–6}. Part of the appeal is its wide range of applicability in explaining phenomena from the natural world and technology, including flashing fireflies^{7,8}, circadian rhythms^{9,10}, neuronal networks¹¹, power-grid networks¹², planar vehicle coordination^{13,14}, etc. The Kuramoto model addresses this diversity of topics by capturing essential aspects of weakly coupled oscillators¹¹, while still being analytically and numerically tractable.

Many extensions of the Kuramoto model have been proposed. Some bridged the Kuramoto model into the field of network theory^{15–19}, extending it from complete graphs to complex networks^{3,4}. A key question in this context is how the structure of the network affects the onset of synchronization⁴. For instance, Watts and Strogatz showed that synchronization is ameliorated by the small-world property of networks^{20,21}. Moreover, it was demonstrated that scale-free networks re-synchronize efficiently after small perturbations²². Other topics of interest include characterizing the equilibria of the homogeneous network Kuramoto model (i.e., with identical natural frequencies) and their basin of attraction by theoretical and numerical means^{23,24}.

Most generalizations assign a single degree of freedom to each oscillator, but there are exceptions where the oscillators evolve on nonlinear manifolds^{25–31}. Such extensions are partly motivated by curiosity, e.g., the swarmalators²⁹ or theoretical results on geometric aspects of synchronization³², and partly to address applications like rigid-body attitude synchronization of robot swarms³³. In particular, the generalized n -sphere model provides a unified framework for the heading orientation on S^1 , the pointing orientation on S^2 , and the full attitude of any rigid-body on $SO(3)$ using a map from the unit quaternions on S^3 . The n -sphere Kuramoto model also appears in quantum synchronization on the Bloch sphere^{27,34}, in opinion consensus dynamics³⁵, and in computer science applications^{36–38}.

In this paper, we complement the previous literature by investigating the global convergence of network Kuramoto models on nonlinear manifolds. Our model extends the n -dimensional sphere Kuramoto model considered by Chandra, Girvan, and Ott^{39–41} to complex networks on ellipsoids. Like them³⁹, we find qualitative differences in the systems depending on the dimension n of the sphere. Moreover, like them⁴¹, we address the instability of incoherent equilibria but for finite networks rather than in thermodynamic limit $N \rightarrow \infty$. We further characterize the convergence properties. For $n \geq 2$, i.e., for all dimensions except that of the standard Kuramoto model ($n = 1$ in our notation), we find that the systems asymptotically converges to synchronization almost globally (i.e., from almost all initial conditions), provided that the spread of the frequency matrices is sufficiently small in the norm. Moreover, for frequency matrices that are all aligned and of even dimension n , we show the asymptotical stability of a single point in the null space of the frequency matrices. These two findings contrast with the standard network Kuramoto model, which has multiple stable equilibrium sets^{23,24} and can only reach phase synchronization in the homogenous case, where all-natural frequencies are identical³. Hence, we show that the generalized network Kuramoto model displays more coherent behavior than the standard model, an appealing property in systems such as groups of animals, and for robust and reliable performance in robot control.

Results and discussion

Kuramoto models. Kuramoto first proposed a network of N harmonic oscillators on a plane, each with a natural frequency ω_i ⁵. An uncoupled oscillator satisfies $\ddot{x}_i = \omega_i^2 x_i$. Set $x_i = \cos \theta_i$ for unit amplitudes and phase angle θ_i , then $\dot{\theta}_i = \omega_i$. The standard Kuramoto model of a complex network of coupled oscillators is given by

$$\dot{\theta}_i = \omega_i + \sum_{j=1}^N k_{ij} \sin(\theta_j - \theta_i), \quad (1)$$

where $i = 1, \dots, N$ and k_{ij} is the coupling strength between oscillator i and j . The coupling parameters k_{ij} are weakly positive and symmetric, $k_{ij} = k_{ji} \geq 0$. The network is recovered from k_{ij} as a graph $\mathcal{G} = (\mathcal{V}, \mathcal{E})$ where the nodes are the oscillators and the edges are node pairs with strictly positive coupling k_{ij} .

The Kuramoto model is usually expressed in polar coordinates as in Eq. (1) but it can also be formulated in Cartesian coordinates $\mathbf{x}_i = [\cos \theta_i \sin \theta_i]^T \in \mathbb{R}^{n+1}$, where $n = 1$ is the dimension of the circle, which yields the dynamics

$$\dot{\mathbf{x}}_i = \Omega_i \mathbf{x}_i + (\mathbf{I}_{n+1} - \mathbf{x}_i \mathbf{x}_i^T) \sum_{j=1}^N k_{ij} \mathbf{x}_j. \quad (2)$$

where the matrix $\Omega \in \mathbb{R}^{(n+1) \times (n+1)}$ is skew-symmetric. The Kuramoto model in Eq. (2) can easily be generalized. By changing the dimensions n to any strictly positive integer, we obtain $\mathbf{x}_i \in \mathbb{R}^{n+1}$ with $\|\mathbf{x}_i\|_2 = 1$ and Ω_i as a skew-symmetric $(n+1) \times (n+1)$ matrix. This yields the n -dimensional network Kuramoto model.

For further perspective on the generalizations of Eq. (2), we consider the network Kuramoto model with homogeneous frequencies on the n -sphere. It is derived from Eq. (2) with $\Omega_i = \Omega_j = \Omega$ for all $\{i, j\} \in \mathcal{E}$. In this special case, like for the standard network Kuramoto model with homogenous frequencies, there is no loss of generality in setting $\Omega_i = \mathbf{0}$. In the following, we refer to this system as the homogeneous model. Note that the agent dynamics still differ with respect to k_{ij} , which compose the effect of the network. The standard homogeneous (and heterogeneous) Kuramoto model can be interpreted as a gradient descent flow^{42,43}. The homogeneous Kuramoto model on S^n can also be interpreted as a gradient descent flow on the sphere surface:

$$\dot{\mathbf{x}}_i = -\mathbf{P}(\mathbf{x}_i) \frac{\partial V}{\partial \mathbf{x}_i} = (\mathbf{I}_{n+1} - \mathbf{x}_i \mathbf{x}_i^T) \sum_{j=1}^N k_{ij} \mathbf{x}_j \quad (3)$$

$$V = \frac{1}{2} \sum_{i,j=1}^N k_{ij} \|\mathbf{x}_i - \mathbf{x}_j\|^2 = \sum_{i,j=1}^N k_{ij} (1 - \mathbf{x}_i \cdot \mathbf{x}_j),$$

where $\mathbf{P}(\mathbf{x}_i) : \mathbb{R}^{n+1} \rightarrow \mathbb{T}_{\mathbf{x}_i} S^n : \mathbf{v} \mapsto (\mathbf{I}_{n+1} - \mathbf{x}_i \mathbf{x}_i^T) \mathbf{v}$ is an orthogonal projection on the tangent space $\mathbb{T}_{\mathbf{x}_i} S^n$ of the n -sphere at \mathbf{x}_i , and V is a potential function that measures the distance to the synchronized state.

Eq. (3) allows us to consider the natural frequency terms Ω_i in Eq. (2) as perturbations of a homogeneous model obtained when all frequencies are equal. The advantage of such an approach is that we can use the large arsenal of tools from the optimization that are available for studying gradient descent flows. This idea leads to our main result, which is valid for frequencies Ω_i that have a small spread around their mean frequency $\frac{1}{N} \sum_{i=1}^N \Omega_i$. This approach has also allowed us to generalize Eq. (3) to a large number of spaces including the Stiefel manifold⁴⁴ and general Riemannian manifolds⁴⁵.

We remark on a third generalization of the Kuramoto model which turns out to be equivalent to the n -sphere model. It is easily

verified that for any $\mathbf{y}_i \in \mathcal{E}^n = \{\mathbf{z} \in \mathbb{R}^{n+1} \mid \mathbf{z}^\top \mathbf{A} \mathbf{z} = 1\}$, the ellipsoid \mathcal{E}^n is invariant under

$$\dot{\mathbf{y}}_i = \Omega_i \mathbf{A} \mathbf{y}_i + (\mathbf{I}_{n+1} - \mathbf{y}_i \mathbf{y}_i^\top \mathbf{A}) \sum_{j=1}^N k_{ij} \mathbf{y}_j, \quad (4)$$

see ref. 46. The change of variables $\mathbf{x}_i = \mathbf{L}^\top \mathbf{y}_i$, where \mathbf{L} is obtained from the Cholesky decomposition $\mathbf{A} = \mathbf{L} \mathbf{L}^\top$, reduces Eq. (4) to Eq. (2) with Ω_i replaced by $\mathbf{L}^\top \Omega_i \mathbf{L}$, see Supplementary Note 1 for details. Hence, results about the sphere model in Eq. (2) also apply to the ellipsoid model in Eq. (4).

Practical synchronization. We define all equilibria that are contained in an open hemisphere as practically synchronized. We refer to the other equilibria as dispersed, see Figs. 1 and 2 for examples. Open hemispheres are geodesically convex sets, i.e., each pair of points in an open hemisphere are connected by a unique geodesic (a great circle). Open hemispheres are the largest subsets of the n -sphere with this property. In particular, open hemispheres are topologically equivalent to Euclidean space \mathbb{R}^n . Many results about the generalized Kuramoto model implicitly utilize this property^{28,47}. The global analysis of dispersed

equilibria, as carried out in this paper, is challenging since it cannot rely on a reduction of a subset of the n -sphere to \mathbb{R}^n .

Our main results establish that any dispersed equilibrium point of Eq. (2) is unstable in the sense of Lyapunov. Practical synchronization yields convergence to the desired set, i.e., synchronization⁴⁸. Since all other equilibria are unstable, over time almost all trajectories turn to practically synchronized configurations. Most of the trajectories which originate near dispersed equilibria diverge from them. The only exceptions are the equilibria themselves and their (small) basins of attraction. The set \mathcal{N} of dispersed equilibria and their basins of attraction have measure zero on $(S^n)^N$. This implies that an initial condition that is uniformly distributed on $(S^n)^N$ has zero probability of being in \mathcal{N} .

In order for our main results to hold, we require that the spread of frequencies Ω_i is small in the following sense:

$$\left(\sum_{i=1}^N \|\Omega_i - \frac{1}{N} \sum_{j=1}^N \Omega_j\|_2^2 \right)^{\frac{1}{2}} < \sum_{(i,j) \in \mathcal{E}} \frac{2K}{N(n+1)} (n-1 - \mathbf{x}_i \cdot \mathbf{x}_j) \cdot (1 - \mathbf{x}_i \cdot \mathbf{x}_j) \quad (5)$$

where $K = \min_{(i,j) \in \mathcal{E}} k_{ij}$ and $n \geq 2$. The dependence of the bound in

Eq. (5) on $(\mathbf{x}_i)_{i=1}^N$ can be removed. To do this, for dispersed configurations $(\mathbf{x}_i)_{i=1}^N$, consider the left-hand side of Eq. (5): it can be upper bounded by a constant, obtained by replacing $\mathbf{x}_i \cdot \mathbf{x}_j$ in the right-hand side by $\cos \pi/N$. The value $\mathbf{x}_i \cdot \mathbf{x}_j = \cos \pi/N$ is found through optimization as explained in Supplementary Note 4. It holds for a path graph with N nodes that are connected as an arc. This arc minimizes the bound in Eq. (5) for dispersed configurations, while the total angle between agents satisfies $\sum_{i=1}^N \arccos \mathbf{x}_i \cdot \mathbf{x}_j = \pi$. Note that the condition Eq. (5) holds for the homogeneous model Eq. (3) except for phase synchronization³³.

Interpretation. The result in Eq. (5) is surprising in light of what we know about the standard network Kuramoto model Eq. (1). Recall that Eq. (1) is multistable and has many other stable equilibrium sets besides synchronization²³. These include the set

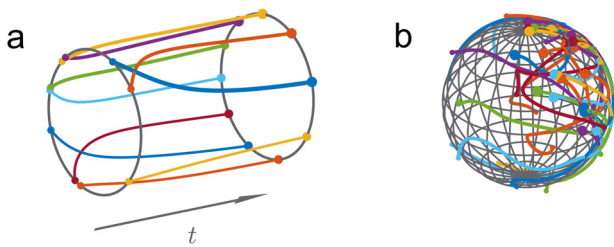


Fig. 1 Spaghetti plots of agent trajectories. Initial and end configurations are indicated by small and large dots, respectively. **a** 10 agents of the homogeneous model, Eq. (3), on the circle S^1 , converge to a 1-twisted state (a dispersed equilibrium) from a random initial condition, see Eq. (6). **b** 20 agents of the heterogeneous model, Eq. (2), on the sphere S^2 converge to practical synchronization from initial conditions given by a dodecahedron configuration.

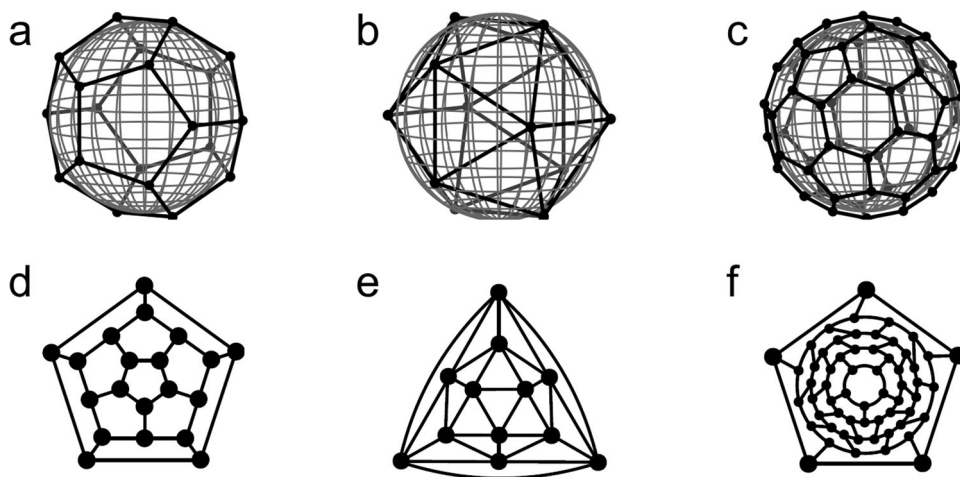


Fig. 2 Dispersed agent configurations and their corresponding graphs. **a-c** Points and bold lines represent the vertices and the edges in the graphs, respectively. The network configurations on the sphere S^2 correspond to Platonic solids **a** dodecahedron and **b** icosahedron. The geometrical configuration of Buckminsterfullerene molecules in **c** corresponds to the Archimedean solid truncated icosahedron. These configurations are obtained when the coupling parameters $k_{ij} \in \{0, K\}$, i.e., the coupling is uniform apart from its dependence on the network, and the network structure is given by the graphs in **d-f**. When the graph is given by one of **d-f** and the agents are in the corresponding dispersed configuration in **a-c**, then this is an unstable equilibrium of the homogeneous Kuramoto model Eq. (3).

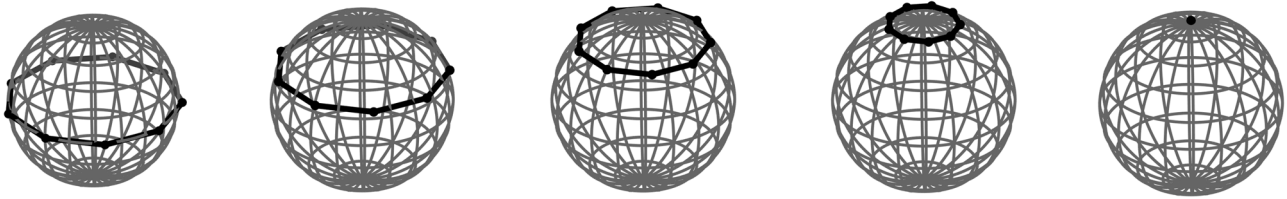


Fig. 3 Convergence to synchronization. Evolution of a configuration with 9 agents connected by a cycle graph on the sphere S^2 . The configuration is continuously deformed from the equator into a point on the north pole (i.e., synchronization) by letting the latitude parameter s in the map given by (Eq. 9) decrease from $s = \pi/2$ to $s = 0$. An equivalent version of this continuous deformation is not possible for the standard Kuramoto model since the circle is a simply connected manifold.

of q -twisted configurations of the homogeneous model Eq. (3), given by

$$\mathcal{T}_q^1 = \{(\theta_i)_{i=1}^N \subset (-\pi, \pi] \mid \theta_i = \phi + 2qi\pi/N, \phi \in \mathbb{R}\}, \quad (6)$$

where the network is given by a cycle graph

$$C_N = (\{1, \dots, N\}, \{\{1, 2\}, \{2, 3\}, \dots, \{N, 1\}\}). \quad (7)$$

On the 2-sphere, we can define q -twisted configurations as equilibria of the homogeneous network Kuramoto model:

$$\mathcal{T}_q^2 = \{(\mathbf{x}_i)_{i=1}^N \subset \mathbb{R}^{n+1} \mid \mathbf{x}_i = \mathbf{R}\mathbf{x}_{i+1}\}$$

where \mathbf{R} is a rotation by $2q\pi/N$ around a vector perpendicular to $\{\mathbf{x}_1, \dots, \mathbf{x}_N\}$, and addition of subindices is modulo N . In contrast to the q -twisted equilibria of the standard model²³, our main result implies that \mathcal{T}_q^2 is an unstable equilibrium manifold of limited interest.

Since q -twisted configurations defined by \mathcal{T}_q^2 are unstable equilibria of Eq. (2), one might conjecture that, on the 2-sphere, there exist other configurations with analogous properties. The q -twisted configurations have the geometric appearance of regular polygons so regular polyhedra may be the equivalent of q -twisted configurations on the 2-sphere. Candidates for such configurations are the Platonic solids (the convex regular polyhedra in \mathbb{R}^3) and Archimedean solids, as well as polyhedra corresponding to molecules of the fullerene family⁴⁹. These configurations can be inscribed in a 2-sphere, such that their vertices lie on the sphere surface, see Fig. 2. Moreover, their edges have a certain symmetry that makes the configurations into equilibria of the homogeneous model Eq. (3), i.e., the sum of agent positions $\sum_{\{i,j\} \in \mathcal{E}} k_{ij} \mathbf{x}_j$ projected on the tangent space $T_{\mathbf{x}_i} S^n$ is zero. By continuity of solutions⁵⁰, there exist perturbed versions of these configurations that are equilibria of the heterogeneous model. However, our main result implies that they are unstable provided (Eq. 5) is satisfied.

To understand why there is a difference between the cases of $n = 1$ and $n \geq 2$, it helps to consider the homogeneous model Eq. (3). Since the flow evolves along the negative gradient of V , it follows that V is decreasing with time. Also note that for $k_{ij} \neq 0$, by definition of V ,

$$\frac{1}{2} \|\mathbf{x}_i - \mathbf{x}_j\|^2 = (1 - \mathbf{x}_i \cdot \mathbf{x}_j) \leq \frac{1}{k_{ij}} V.$$

Let us consider a 1-twisted configuration on the circle or 2-sphere, i.e., $(\theta_i)_{i=1}^N \in \mathcal{T}_1^1$ or $(\mathbf{x}_i)_{i=1}^N \in \mathcal{T}_1^2$. Then V is a sum of circle chord lengths, $V = N \sin^2 \pi/N \rightarrow 0$ as $N \rightarrow \infty$. This implies that

$$1 - \cos(\theta_i(t) - \theta_j(t)) \leq \frac{1}{k_{ij}} N \sin^2 \pi/N \quad (8)$$

holds for all future times $t \in [0, \infty)$. In particular, for the standard Kuramoto model to go from a configuration in \mathcal{T}_q^1 to a

synchronized state, there must be a time τ and a pair of oscillators that satisfy $|\theta_i(\tau) - \theta_j(\tau)| = \pi$. This is not possible for large N , as it would contradict Eq. (8).

Consider instead a configuration $(\mathbf{x}_i)_{i=1}^N \in \mathcal{T}_q^2$. The equilibrium $(\mathbf{x}_i)_{i=1}^N$ lies on a great circle, which we without loss of generality assume to be the equator. We can perturb the agents towards the north pole without increasing V . To see this, use spherical coordinates

$$\mathbf{x}_i = \begin{bmatrix} x_i \\ y_i \\ z_i \end{bmatrix} = \begin{bmatrix} \sin \theta_i \cos \phi_i \\ \sin \theta_i \sin \phi_i \\ \cos \theta_i \end{bmatrix} = \begin{bmatrix} \sin s \cos 2\pi i/N \\ \sin s \sin 2\pi i/N \\ \cos s \end{bmatrix}. \quad (9)$$

By decreasing the s parameter from $\pi/2$ at the equator to 0 at the north pole we continuously deform the great circle into a point while staying on the sphere, see Fig. 3. The value of the potential function strictly decreases: $V = 4N \sin s \sin^2 \pi/N \rightarrow 0$ as $s \rightarrow 0$.

For a more intuitive understanding of this result, let again the graph be the cycle given by Eq. (7). We may consider the agents as beads on a string, where each bead is an agent and the string is composed of all pairwise geodesic curves (great circles) that connect any two neighboring agents. This idea is valid in the much more general setting of gradient descent flows like Eq. (3) on Riemannian manifolds \mathcal{M} ⁴⁵. These flows are generalizations of the homogeneous Kuramoto model with zero natural frequencies. The fact that V is decreasing can again be used to bound $\|\mathbf{x}_i - \mathbf{x}_{i+1}\|$. For sufficiently small agent distances, the pairwise geodesics are unique and change continuously. This implies that the string, i.e., the closed curve composed of all pairwise geodesics, changes continuously. If \mathcal{M} is multiply connected, then by definition of this property, there exists at least one closed curve which cannot be continuously deformed to a point. Hence we only need to choose our initial conditions so that the string approximates this curve and the topology of the manifold will prevent synchronization.

The manifold property of being simply connected versus multiply connected is one thing that distinguishes the circle from all other spheres (we do not consider the 0-sphere $S^0 = \{-1, 1\}$). The circle is multiply connected since it cannot be continuously deformed to a point. The spheres are simply connected since any closed curve can be continuously deformed to a point as we did with the equator in Eq. (9) and Fig. 3. In this sense, synchronization on the circle is more similar to synchronization on $SO(n)$, which is multiply connected, than to synchronization on S^n . Note that the two manifolds are diffeomorphic $S^1 \cong SO(2)$ through the linear map

$$\mathbf{f} : S^1 \rightarrow SO(2) : \begin{bmatrix} \cos \theta_i \\ \sin \theta_i \end{bmatrix} \mapsto \begin{bmatrix} \cos \theta_i & -\sin \theta_i \\ \sin \theta_i & \cos \theta_i \end{bmatrix}.$$

Phase synchronization. We have a second result that applies to spheres S^n of even dimension n . Define convergence to a point,

i.e., $\mathbf{x}_i = \mathbf{x}_j$ for all $\{i, j\}$ in \mathcal{E} , as phase synchronization. We show that phase synchronization is possible on \mathcal{S}^n in the case of nonidentical natural frequencies. Like our first result Eq. (5), this finding distinguishes the network Kuramoto model on \mathcal{S}^1 and \mathcal{S}^2 . Phase synchronization on \mathcal{S}^1 requires identical natural frequencies, $\omega_i = \omega_j$ for all $\{i, j\}$ in \mathcal{E} . A key difference between this result and Eq. (5) is that it does not constrain the magnitude of the frequency norms in any way. However, like the findings of^{39,51} it depends on the parity of the dimension n of the sphere.

Let $\ker \Omega_i$ denote the null space of the natural frequency matrix Ω_i . If there exists a nonzero vector \mathbf{v} such that

$$\text{span}\{\mathbf{v}\} = \bigcap_{i=1}^N \ker \Omega_i \tag{10}$$

then for any initial condition which satisfies

$$\{\mathbf{x}_1 \dots \mathbf{x}_N\} \subset \mathcal{H}^n(\mathbf{v}) = \{\mathbf{x} \in \mathcal{S}^n \mid \mathbf{v} \cdot \mathbf{x} > 0\}, \tag{11}$$

it holds that $\mathbf{x}_i \rightarrow \mathbf{v}$ as $t \rightarrow \infty$. Moreover, \mathbf{v} is an asymptotically stable equilibrium. Note that if the frequency matrices satisfy the synchronization condition given by our result, Eq. (5), then the convergence to phase synchronization is almost global. Simulations also indicate that condition (Eq. 11) is redundant. To understand why it's needed for the proof, see Supplementary Note 5. To interpret the synchronization condition, consider the 2-sphere. If e.g., we chose $\mathbf{v} = \mathbf{e}_3$, it means $\Omega_i \mathbf{x}_i = \omega_i \mathbf{v} \times \mathbf{x}_i$, where $\omega_i \in \mathbb{R}$. Initialize all agents in the northern hemisphere, then all agents converge to phase synchronization in the north pole. Note that a random $\Omega_i \in \text{SO}(n+1)$ has full rank if n is odd, whereby $\mathbf{v} = \mathbf{0}$ and (Eq. 11) cannot hold. For even n however, the dimension of $\ker \Omega_i$ is always at least 1.

It should be noted that condition (Eq. 10) refers to a special case that would not appear if the frequency matrices are selected uniformly at random. Rather, it suggests that all frequency matrices are in a sense somewhat similar. This may occur in a real-world system where the drift term in Eq. (2) is due to an exterior cause. For example, if the agents are fish they may be caught in a stream, or if they are drones the external influence could be wind. Such situations can also be modeled by our assumption (Eq. 5) which assumes the frequencies have a small spread around a large mean value. Another scenario is a single agent with a nonzero frequency matrix, perhaps due to a malfunction in an otherwise homogeneous robotic system. From a theoretical perspective, condition (Eq. 10) is interesting as a counterexample to what one might assume based on the standard Kuramoto model since it shows a counter-intuitive property of the high-dimensional model.

To understand the mechanics behind the result (Eq. 11), it is helpful to consider a two-agent case on \mathcal{S}^2 ,

$$\begin{aligned} \dot{\mathbf{x}}_1 &= \Omega_1 \mathbf{x}_1 + (\mathbf{I}_{n+1} - \mathbf{x}_1 \mathbf{x}_1^\top) k_{12} \mathbf{x}_2, \\ \dot{\mathbf{x}}_2 &= (\mathbf{I}_{n+1} - \mathbf{x}_2 \mathbf{x}_2^\top) k_{12} \mathbf{x}_1, \end{aligned} \tag{12}$$

where Ω_1 yields a rotation around the vector \mathbf{e}_3 . Consider three cases: (i) If the agents are in sync, then agent 2 will break away from agent 1 due to the drift term $\Omega_1 \mathbf{x}_1$. The only exception to this is if \mathbf{x}_1 belongs to $\ker \Omega_1$, i.e., $\mathbf{x}_1 = \mathbf{e}_3$; (ii) If the agents are on different latitudes $\theta_1 \neq \theta_2$ in the spherical coordinates Eq. (9), then the latitude θ_i of the agent i with the lowest latitude will increase. In sum, the agent with the lowest latitude θ_i moves closer to \mathbf{e}_3 ; (iii) If the agents have the same latitude $\theta_1 = \theta_2$, then the drift term $\Omega_1 \mathbf{x}_1$ in the dynamics of agent 1 will cause it to rotate at this latitude. However, both agents will also move closer to the north pole. This is due to the coupling terms being aligned with the tangent space of the great circle connecting the two agents (see Fig. 4). The great circle connecting two points of the

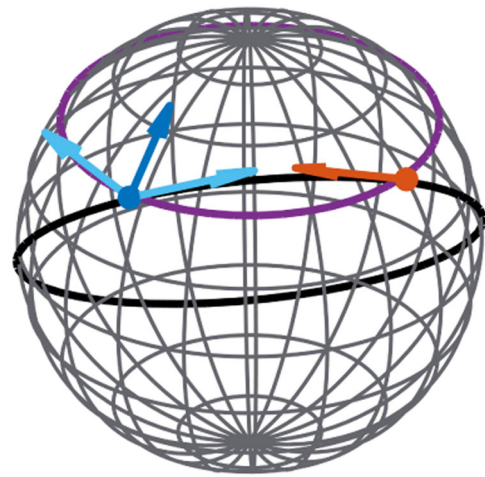


Fig. 4 Positions and velocities in a two-agent system on the sphere \mathcal{S}^2 .

One agent has clockwise drift around the z-axis (blue dot) and the other agent is without drift (red dot). The two agents are situated at the same latitude (purple circle). However, the coupling terms in the dynamics are tangent to the great circle connecting both agents (black). The dark blue vector is the sum of light blue vectors. The time derivatives of both agents (dark blue and red arrows) are pointing north of the latitude on which the agents lie. Hence, the latitudes are increasing.

same latitude has a segment at a higher latitude than the common latitude of the two points themselves.

Simulations

Practical synchronization. We are interested in how geometric and topological properties of the manifold affect the convergence of Kuramoto models. To this end, we study a large family of manifolds that include the n -spheres, the generalizations of $\mathcal{S}^1 \cong \text{SO}(2)$ to the special orthogonal group $\text{SO}(n)$, and other manifolds in-between. This family is the Stiefel manifolds $\text{St}(p, n)$ defined by

$$\text{St}(p, n) = \{\mathbf{S} \in \mathbb{R}^{n \times p} \mid \mathbf{S}^\top \mathbf{S} = \mathbf{I}_p\},$$

where $p \leq n$. The Stiefel manifolds are rectangular orthogonal matrices; the manifold $\text{St}(p, n)$ is composed of the first p columns of all orthogonal matrices $\mathbf{Q} \in \text{O}(n)$. The following diffeomorphisms show the versatility of the Stiefel manifold framework $\text{St}(1, n+1) \cong \mathcal{S}^n$, $\text{St}(n-1, n) \cong \text{SO}(n)$, and $\text{St}(n, n) \cong \text{O}(n)$. The Kuramoto model on Stiefel manifolds can be obtained as a generalization of the gradient flow formulation for the n -sphere model, Eq. (3). Along those lines, the following model is introduced in⁴⁴:

$$\dot{\mathbf{S}}_i = -\mathbf{P}(\mathbf{S}_i) \frac{\partial V}{\partial \mathbf{S}_i} \tag{13}$$

$$= \mathbf{S}_i \text{skew} \left(\mathbf{S}_i^\top \sum_{j=1}^N k_{ij} \mathbf{S}_j \right) + (\mathbf{I}_{n+1} - \mathbf{S}_i \mathbf{S}_i^\top) \sum_{j=1}^N k_{ij} \mathbf{S}_j,$$

$$V = \frac{1}{2} \sum_{i,j=1}^N k_{ij} \|\mathbf{S}_i - \mathbf{S}_j\|^2 = \sum_{i,j=1}^N k_{ij} (p - \mathbf{S}_i^\top \mathbf{S}_j).$$

Eq. (13) can be expressed as a coupled oscillator system by the addition of frequency terms,

$$\dot{\mathbf{S}}_i = \Omega_i \mathbf{S}_i + \mathbf{S}_i \Xi_i - \mathbf{P}(\mathbf{S}_i) \frac{\partial V}{\partial \mathbf{S}_i}, \tag{14}$$

where $\Omega \in \text{SO}(n)$, $\Xi \in \text{SO}(p)$. See refs. ^{44,52} for more details.

Table 1 Probability of convergence to synchronization from a random initial condition.

	<i>n</i>								
	1	2	3	4	5	6	7	8	9
1	0.06	0.95	1	1	1	1	1	1	1
2		0.05	0.92	1	1	1	1	1	1
3			0.06	0.92	1	1	1	1	1
4				0.05	0.91	1	1	1	1
<i>p</i> 5					0.06	0.89	1	1	1
6						0.05	0.90	1	1
7							0.06	0.90	1
8								0.06	0.90
9									0.06

Probability measure, $\mu(\mathcal{B}(\mathcal{S})) \in [0, 1]$, of the basin of attraction $\mathcal{B}(\mathcal{S})$ of the sync manifold \mathcal{S} on the Stiefel manifold $\text{St}(p, n)$ with parameters p, n for a cycle network with 5 agents given by the graph \mathcal{C}_5 defined by Eq. (7). The calculation of $\mu(\mathcal{B})$ is done by Monte Carlo integration using $M = 10^4$ samples of the uniform distribution on $\text{St}(p, n)$ for each pair (p, n) , see “Methods” section for details. We set the threshold value $\epsilon = 0.01$ in Eq. (20) and the final time $T = 200$. Rows in the table fix p , columns fix n . An empty cell indicates that there is no Stiefel manifold for that pair (p, n) . Bold font indicates that (p, n) satisfies $\frac{2}{3}n - 1 < p \leq n - 2$ whereby our previous result⁴⁴ does not apply.

For the homogeneous model, we are interested in the measure $\mu(\mathcal{B}(\mathcal{S}))$ of the basin of attraction $\mathcal{B}(\mathcal{S})$ of the synchronization manifold \mathcal{S} . To find an equivalent of $\mu(\mathcal{B}(\mathcal{S}))$ for practical synchronization we introduce an order parameter

$$\mathbf{R} = \frac{1}{Np} \sum_{i=1}^N \mathbf{S}_i. \tag{15}$$

The factor $1/p$ ensures that $R = \|\mathbf{R}\|_F = 1$ when all matrices are equal, $\mathbf{S}_i = \mathbf{S}_j$ for all $\{i, j\} \in \mathcal{E}$. By taking the average value of \mathbf{R} at a large time T over many simulations we get an index of convergence to synchronization for Eq. (14) that is similar to what $\mu(\mathcal{B}(\mathcal{S}))$ is for Eq. (13). Note that \mathbf{R} is a generalization of the order parameter of the standard Kuramoto model on \mathcal{S}^{13} .

The details of numerical integration of Eq. (13) are given in the “Methods” section. Results of the simulation are displayed in Table 1. Note that almost global convergence to synchronization on $\text{St}(p, n)$ is observed for pairs (p, n) that satisfy $p \leq n - 2$. That almost global convergence holds for pairs that satisfy $p \leq 2n/3 - 1$ has been proved analytically⁴⁴. However, we conjecture that it also holds for $p \leq n - 2$, which corresponds to all the simply connected Stiefel manifolds⁵³. As we argued in the *Interpretation* section based on ref. 45, almost global convergence for all connected graphs is impossible on a manifold that is multiply connected. Failures to reach consensus occur when $p \in \{n - 1, n\}$, i.e., for the special orthogonal group and the orthogonal group. For the case of $\mathcal{O}(n)$, the probability that all agents belong to the same connected component ($\det \mathbf{Q} = 1$ or $\det \mathbf{Q} = -1$) is $2^{-4} \approx 0.06$, which explains the numbers on the diagonal where $p = n$.

Many results that guarantee synchronization on nonlinear space are limited to geodesically convex sets, e.g., hemispheres of the n -sphere^{28,47,48,54}. This does not scale well for large N since the probability that all N agents belong to a hemisphere decreases exponentially with N . However, even though a theoretical guarantee does not scale well, actual system performance may still do. This is the case on \mathcal{S}^n for $n \in \mathbb{N} \setminus \{1\}$ for the homogeneous model since \mathcal{S} is almost globally stable³³.

It is of interest to investigate how $\mu(\mathcal{B})$ scales with N when the consensus manifold is not almost globally stable. Figure 5 reveals that on $\text{St}(1, 2) \cong \mathcal{S}^1$, $\mu(\mathcal{B})$ decreases steadily with N (see also ref. 23). On $\text{St}(2, 3) \cong \text{SO}(3)$, $\text{St}(3, 4) \cong \text{SO}(4)$, and $\text{St}(4, 5) \cong \text{SO}(5)$ the value of $\mu(\mathcal{B})$ settles on 0.5. Note that there is not any immediate reason to expect that $\lim_{N \rightarrow \infty} \mu(\mathcal{B})$ even exists. For

each $N = 5k$, where $k \in \mathbb{N}$, there is a new q -twisted equilibrium set that is stable on $\text{St}(n - 1, n)$. However, there does not appear to be any large difference between $\mu(\mathcal{B})$ when $N = 5k$ for $k \in \mathbb{N}$ compared to $N - 1$ except for the case of $N = 5$. The size of $\text{St}(p, n)^N$ grows with N . The average time required to satisfy our simulation termination criteria increases with N . This introduces a dependence on N in the bias towards underestimating $\mu(\mathcal{B})$, but the effect is small as we have investigated by increasing the termination time T .

We compare the size of the synchronization basin, $\mu(\mathcal{B}(\mathcal{S}))$ with the average order parameter from M simulations, $1/M \sum_{i=1}^M \mathbf{R}$, see Fig. 5. The way the μ and R curves depend on the number of agents N are strikingly similar. Inspect condition Eq. (5) for $n = 2$, a network given by the cycle graph \mathcal{C}_N , and a constant RHS obtained by setting $\langle \mathbf{x}_i, \mathbf{x}_j \rangle = \cos \pi/N$. This yields

$$\left(\sum_{i=1}^N \|\Omega_i - \frac{1}{N} \sum_{j=1}^N \Omega_j\|_2^2 \right)^{\frac{1}{2}} < \frac{2K}{3} \left(1 - \cos \frac{\pi}{N} \right)^2$$

which suggest that Ω_i should scale as $\mathcal{O}(K/N^4)$. However, the use of $\langle \mathbf{x}_i, \mathbf{x}_j \rangle = \cos \pi/N$ in the condition is conservative since it is derived for a worst-case scenario. In simulations, we find that scaling Ω_i as $1/N$ suffices to approximately replicate the $\mu(\mathcal{B}(\mathcal{S}))$ curves, see Fig. 5.

Phase synchronization. We use simulations to study the order parameter R given by Eq. (15) as a function of the coupling parameters $K = \min_{(i,j) \in \mathcal{E}} k_{ij}$ under the assumptions of the synchronization condition in Eq. (10). We draw Ω_1 such that $(\Omega_1)_{st} \in N(1, 1)$ if $s < t$ and $(\Omega_1)_{st} \in N(-1, 1)$ if $s > t$. Then we set $\Omega_i = \omega_i \Omega_1$ where $\omega_i \in N(0, 1)$ for $i = 2, \dots, N$. Generically, this results in skew-symmetric matrices of maximal rank. However, that means $\text{rank } \Omega_i = n$ for even n and $\text{rank } \Omega_i = n + 1$ for odd n . In particular, this implies the existence of a \mathbf{v} satisfying Eq. (10) for even n but not for odd n . We find that it is not necessary to limit the initial conditions to a hemisphere as we required for our analytic result; the simulated system is observed to converge to phase synchronization from (almost) all initial conditions if a single joint nullspace vector exists. We use the complete graph $\mathcal{G} = \mathcal{K}_N$ since it allows for a comparison of our findings with similar results in refs. 39,51. For this reason, we also use the normalization factor $1/N$ in front of the coupling terms in Eq. (2). In particular, we find that the phase transition from disorder to synchronization is explosive and discontinuous for even n but not for odd n where it is continuous, see Fig. 6. We expected this difference based on Eq. (10) since the full rank of generic skew-symmetric matrices with even dimension $n + 1$ (the dimension of the matrix, not the sphere) prevents condition Eq. (10) from applying. We also find that practical synchronization holds when small perturbations are added to each of the frequency matrices (note that the condition of Eq. (5) does not need to be satisfied).

Methods

Proof sketch. A full derivation of the result in Section “Practical synchronization” is given in Supplementary Note 2–4. This section provides a brief sketch of the main ideas. For the sake of simplicity, we focus on the stronger assumption

$$\left(\sum_{i=1}^N \|\Omega_i\|^2 \right)^{\frac{1}{2}} < \sum_{(i,j) \in \mathcal{E}} \frac{2K}{N(n+1)} (n - 1 - \cos \pi/N) \cdot (1 - \cos \pi/N). \tag{16}$$

Note that we do not require $\sum_{j=1}^N \Omega_j = \mathbf{0}$ in Eq. (5) for Eq. (16) to hold, rather we just let each Ω_i be small in the norm.

Our approach is based on a matrix perturbation result⁵⁵ that relates the spectrum of three matrices. Let $\mathbf{A}(\mathbf{x})$ and $\mathbf{B}(\mathbf{x})$ be the linearization matrices of (Eq. 2) and its particularization for $\Omega_i = \mathbf{0}$ (respectively) at a dispersed equilibrium $\mathbf{x} = (\mathbf{x}_i)_{i=1}^N$. We bound the spectrum of $\mathbf{A}(\mathbf{x}) = \Omega + \mathbf{B}(\mathbf{x})$, where

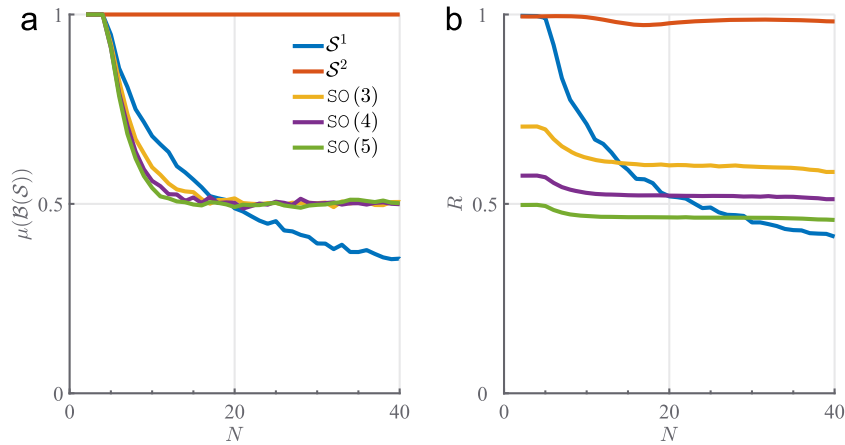


Fig. 5 Indicators of convergence to synchronization and practical synchronization. **a** Probability measure, $\mu(\mathcal{B}(\mathcal{S})) \in [0, 1]$, of the basin of attraction $\mathcal{B}(\mathcal{S})$ of the synchronization manifold \mathcal{S} given by (Eq. 19) on the spheres $\mathcal{S}^1, \mathcal{S}^2$ and Stiefel manifold $\text{St}(n-1, n) \cong \text{SO}(n)$ (special orthogonal group) for $n \in \{3, 4, 5\}$ where the network is given by the graph C_N defined by Eq. (7) and the number of agents $N \in \{2, \dots, 40\}$. The probability measure $\mu(\mathcal{B})$ is calculated by Monte Carlo integration over $M = 10^4$ system evolutions for each point. **b** Average value of the order parameter R given by Eq. (15); each point corresponds to 10^4 simulations. The graph is the cycle graph C_N given by (7). We set the coupling parameters between neighboring agents i and j to $k_{ij} = 1$. The (s, t) -elements of the frequency matrix $(\Omega_i)_{st} \in \mathcal{N}(1, 1/N^2)$ if $s < t$ and $(\Omega_i)_{st} \in \mathcal{N}(-1, 1/N^2)$ if $s > t$, where $\mathcal{N}(\cdot, \cdot)$ denotes a normal distribution.

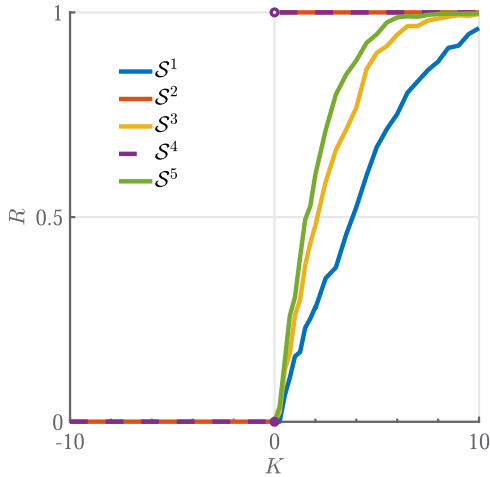


Fig. 6 The transition from incoherence to synchronization depends on the parity (odd/even) of the dimension n of the n -sphere \mathcal{S}^n . The order parameter R is given by Eq. (15). The uniform coupling parameters $k_{ij} = K$ between agent i and j range from negative, where $R = 0$ indicates incoherence, to positive, where $R = 1$ indicates synchronization. We take the average value of R from $M = 10^3$ system evolutions per point. We use $N = 100$ agents. To find the discontinuous phase transition for small K values we have chosen a large final time $T = 2000$.

$\Omega = \text{diag}(\Omega_1, \dots, \Omega_N)$, using skew-symmetry of Ω and symmetry of $\mathbf{B}(\mathbf{x})$. The result on matrix perturbations⁵⁵ yields

$$|\text{Re } \alpha(\mathbf{x}) - \beta(\mathbf{x})| \leq \|\mathbf{A}(\mathbf{x}) - \mathbf{B}(\mathbf{x})\|_2$$

$$= \left(\sum_{i=1}^N \|\Omega_i\|_2^2 \right)^{\frac{1}{2}}, \tag{17}$$

where $\text{Re } \alpha(\mathbf{x})$ and $\beta(\mathbf{x})$ are the eigenvalues with the largest real part of $\mathbf{A}(\mathbf{x})$ and $\mathbf{B}(\mathbf{x})$ respectively.

A lower bound for $\beta(\mathbf{x})$ is known³³. We use techniques from optimization to derive the following inequality which holds at any dispersed equilibrium \mathbf{x} ,

$$\beta(\mathbf{x}) \geq \frac{K}{n+1} \left(n - 1 - \cos \frac{\pi}{N} \right) \left(1 - \cos \frac{\pi}{N} \right). \tag{18}$$

Suppose that the assumption (Eq. 16) holds, then

$$|\text{Re } \alpha(\mathbf{x}) - \beta(\mathbf{x})| \leq \left(\sum_{i=1}^N \|\Omega_i\|_2^2 \right)^{\frac{1}{2}}$$

$$< \frac{K}{n+1} \left(n - 1 - \cos \frac{\pi}{N} \right) \left(1 - \cos \frac{\pi}{N} \right)$$

$$\leq \beta(\mathbf{x}),$$

where we used the result (Eq. 17). From $|\text{Re } \alpha(\mathbf{x}) - \beta(\mathbf{x})| < \beta(\mathbf{x})$ we get $\text{Re } \alpha(\mathbf{x}) > 0$. It follows that the equilibrium \mathbf{x} is exponentially unstable.

Simulations. We perform simulations to investigate how the basin of attraction $\mathcal{B}(\mathcal{S})$ of the synchronization manifold $\mathcal{S} \cong \text{St}(p, n)$ depends on the Stiefel manifold on which a generalized Kuramoto model evolves. Let $\Phi : \mathbb{R} \times \text{St}(p, n)^N \rightarrow \text{St}(p, n)^N$ denote the flow of the homogeneous Kuramoto model, Eq. (13), i.e.,

$$\Phi(t, (\mathbf{S}_i)_{i=1}^N) = (\mathbf{S}_i(t))_{i=1}^N$$

given that $(\mathbf{S}_i(0))_{i=1}^N = (\mathbf{S}_{i,0})_{i=1}^N \in \text{St}(p, n)^N$. Denote $\Phi = (\Phi_i)_{i=1}^N$. Let $\mathcal{B}(\mathcal{S})$ denote the basin of attraction of the synchronization manifold $\mathcal{S} \cong \text{St}(p, n)$,

$$\mathcal{S} = \{(\mathbf{S}_i)_{i=1}^N \in \text{St}(p, n)^N \mid \mathbf{S}_i = \mathbf{S}_j, \forall \{i, j\} \in \mathcal{E}\}, \tag{19}$$

$$\mathcal{B}(\mathcal{S}) = \{(\mathbf{S}_i)_{i=1}^N \in \text{St}(p, n)^N \mid \lim_{t \rightarrow \infty} \Phi(t, (\mathbf{S}_i)_{i=1}^N) \in \mathcal{S}\}.$$

For the heterogeneous model, we have a practical synchronization manifold \mathcal{D} of (14) defined by

$$\mathcal{D} = \left\{ (\mathbf{S}_i)_{i=1}^N \in (\mathcal{S}^n)^N \mid \Omega_i \mathbf{S}_i + \mathbf{S}_i \Xi_i - \mathbf{P}(\mathbf{S}_i) \frac{\partial V}{\partial \mathbf{S}_i} = \mathbf{0} \right\},$$

The existence of such a manifold for sufficiently small Ω_i, Ξ_i follows by a perturbation theory argument⁴⁸.

The probability measure $\mu(\mathcal{B}(\mathcal{S}))$ is the fraction of initial conditions for which the system in Eq. (13) converges to the synchronization manifold \mathcal{S} . The measure $\mu(\mathcal{B}(\mathcal{S}))$ can be calculated by Monte Carlo integration:

$$\frac{1}{M} \sum_{k=1}^M \mathbb{1}_{\mathcal{S}} \left(\lim_{t \rightarrow \infty} \Phi(t, (\mathbf{S}_i^k)_{i=1}^N) \right) \xrightarrow{\text{a.s.}} \mu(\mathcal{B}) \text{ as } M \rightarrow \infty,$$

where $\mathbb{1} : \text{St}(p, n)^N \rightarrow \{0, 1\}$ is the indicator function and $(\mathbf{S}_i^k)_{i=1}^N$ for each $k \in \{1, \dots, M\}$ is a sample drawn from the uniform distribution on $\text{St}(p, n)^N$. A uniform sample \mathbf{S} is found by drawing $\mathbf{X} \in \mathbb{R}^{n \times p}$ such that each element of \mathbf{X} is independent and identically normally distributed $\mathcal{N}(0, 1)$ and forming $\mathbf{S} = \mathbf{X}(\mathbf{X}^T \mathbf{X})^{-\frac{1}{2}}$.

A stop criterion is needed to (approximately) calculate $\lim_{t \rightarrow \infty} \Phi(t, (\mathbf{S}_i)_{i=1}^N)$. The simulation synchronizes if

$$\max_{(j,k) \in \mathcal{E}} \frac{1}{2} \|\Phi_j(T, (\mathbf{S}_i)_{i=1}^N) - \Phi_k(T, (\mathbf{S}_i)_{i=1}^N)\| < \varepsilon \tag{20}$$

for a threshold value $\varepsilon \in (0, \infty)$ at a fixed time T . The tensor $\Phi(T, (\mathbf{S}_{k,0})_{k=1}^N)$ is obtained by integrating Eq. (13) using the function ode45 in MATLAB. If Eq. (20) is satisfied at T , we count this as a case of convergence to \mathcal{S} . There are potential

issues with long simulation times causing numerical errors to accumulate so that either the system leaves the Stiefel manifold or is perturbed from \mathcal{B}° into \mathcal{B} . We have dealt with such issues. In particular, there might be a bias towards underestimating the value of $\mu(\mathcal{B})$ due to $T < \infty$, but the effect is small for large T .

Data availability

The data used in this paper is available from the GitHub account of the corresponding author: <https://github.com/johanmarkdahl/CommPhys2021>. The data is also available on request to the corresponding author.

Received: 21 March 2021; Accepted: 20 July 2021;

Published online: 20 August 2021

References

- Winfree, A. T. Biological rhythms and the behavior of populations of coupled oscillators. *J. Theor. Biol.* **16**, 15–42 (1967).
- Arenas, A., Diaz-Guilera, A., Kurths, J., Moreno, Y. & Zhou, C. Synchronization in complex networks. *Phys. Rep.* **469**, 93–153 (2008).
- Dörfler, F. & Bullo, F. Synchronization in complex networks of phase oscillators: a survey. *Automatica* **50**, 1539–1564 (2014).
- Rodrigues, F. A., Peron, T. K. D., Ji, P. & Kurths, J. The Kuramoto model in complex networks. *Phys. Rep.* **610**, 1–98 (2016).
- Kuramoto, Y. Self-entrainment of a population of coupled non-linear oscillators. In *International Symposium on Mathematical Problems in Theoretical Physics*. 420–422 (Springer, 1975).
- Strogatz, S. H. From Kuramoto to Crawford: exploring the onset of synchronization in populations of coupled oscillators. *Phys. D* **143**, 1–20 (2000).
- Ermentrout, B. An adaptive model for synchrony in the firefly *Pteroptyx malaccaea*. *J. Math. Biol.* **29**, 571–585 (1991).
- Buck, J. & Buck, E. Mechanism of rhythmic synchronous flashing of fireflies: Fireflies of Southeast Asia may use anticipatory time-measuring in synchronizing their flashing. *Science* **159**, 1319–1327 (1968).
- Antonsen, Jr., T., Faghih, R., Girvan, M., Ott, E. & Platig, J. External periodic driving of large systems of globally coupled phase oscillators. *Chaos* **18**, 037112 (2008).
- Childs, L. M. & Strogatz, S. H. Stability diagram for the forced Kuramoto model. *Chaos* **18**, 043128 (2008).
- Hoppensteadt, F. C. & Izhikevich, E. M. *Weakly Connected Neural Networks*, Vol. 126 (Springer Science and Business Media, 2012).
- Dörfler, F., Chertkov, M. & Bullo, F. Synchronization in complex oscillator networks and smart grids. *Proc. Natl Acad. Sci. USA* **110**, 2005–2010 (2013).
- Klein, D. J., Lee, P., Morgansen, K. A. & Javidi, T. Integration of communication and control using discrete time Kuramoto models for multivehicle coordination over broadcast networks. *IEEE J. Sel. Areas Commun.* **26**, 695–705 (2008).
- Sepulchre, R., Paley, D. A. & Leonard, N. E. Stabilization of planar collective motion: all-to-all communication. *IEEE Trans. Autom. Control* **52**, 811–824 (2007).
- Albert, R. & Barabási, A.-L. Statistical mechanics of complex networks. *Rev. Mod. Phys.* **74**, 47 (2002).
- Dorogovtsev, S. N. & Mendes, J. F. Evolution of networks. *Adv. Phys.* **51**, 1079–1187 (2002).
- Newman, M. E. Properties of highly clustered networks. *Phys. Rev. E* **68**, 026121 (2003).
- Barabási, A.-L. Network science. *Philos. T. R. Soc. A* **371**, 20120375 (2013).
- Motter, A. E. Networkcontrolology. *Chaos* **25**, 097621 (2015).
- Watts, D. J. & Strogatz, S. H. Collective dynamics of ‘small-world’ networks. *Nature* **393**, 440–442 (1998).
- Strogatz, S. H. Exploring complex networks. *Nature* **410**, 268–276 (2001).
- Moreno, Y. & Pacheco, A. F. Synchronization of Kuramoto oscillators in scale-free networks. *Europhys. Lett.* **68**, 603 (2004).
- Wiley, D. A., Strogatz, S. H. & Girvan, M. The size of the sync basin. *Chaos* **16**, 015103 (2006).
- Canale, E. A. & Monzón, P. Exotic equilibria of Harary graphs and a new minimum degree lower bound for synchronization. *Chaos* **25**, 023106 (2015).
- Ritort, F. Solvable dynamics in a system of interacting random tops. *Phys. Rev. Lett.* **80**, 6 (1998).
- Olfati-Saber, R. Swarms on sphere: a programmable swarm with synchronous behaviors like oscillator networks. In *Proceedings of the 45th IEEE Conference on Decision and Control*. 5060–5066 (IEEE, 2006).
- Lohe, M. Quantum synchronization over quantum networks. *J. Phys. A* **43**, 465301 (2010).
- Zhu, J. Synchronization of Kuramoto model in a high-dimensional linear space. *Phys. Lett. A* **377**, 2939–2943 (2013).
- O’Keeffe, K. P., Hong, H. & Strogatz, S. H. Oscillators that sync and swarm. *Nat. Commun.* **8**, 1–13 (2017).
- Ha, S.-Y., Ko, D. & Ryoo, S. On the relaxation dynamics of Lohe oscillators on some Riemannian manifolds. *J. Stat. Phys.* **172**, 1427–1478 (2018).
- Ha, S. Y. & Park, H. Emergent behaviors of the generalized Lohe matrix model. *Discrete Contin. Dyn. Syst. B* **26**, 4227–4261 (2021).
- Tron, R., Afsari, B. & Vidal, R. Intrinsic consensus on SO(3) with almost-global convergence. In *Proc. 51st IEEE Conference on Decision and Control (CDC)*. 2052–2058 (IEEE, 2012).
- Markdahl, J., Thunberg, J. & Gonçalves, J. Almost global consensus on the n -sphere. *IEEE Trans. Autom. Control* **63**, 1664–1675 (2018).
- DeVille, L. Synchronization and stability for quantum Kuramoto. *J. Stat. Phys.* **174**, 160–187 (2019).
- Aydo, A., McQuade, S. & Duteil, N. Opinion dynamics on a general compact Riemannian manifold. *Netw. Heterog. Media* **12**, 489–523 (2017).
- Al-Abri, S., Wu, W. & Zhang, F. A gradient-free three-dimensional source seeking strategy with robustness analysis. *IEEE Trans. Autom. Control* **64**, 3439–3446 (2018).
- Crnkčić, A. & Jaćimović, V. Swarms on the 3-sphere with adaptive synapses: Hebbian and anti-Hebbian learning rule. *Syst. Control Lett.* **122**, 32–38 (2018).
- Crnkčić, A. & Jaćimović, V. Data clustering based on quantum synchronization. *Nat. Comput.* **18**, 907–911 (2019).
- Chandra, S., Girvan, M. & Ott, E. Continuous versus discontinuous transitions in the D -dimensional generalized Kuramoto model: Odd D is different. *Phys. Rev. X* **9**, 011002 (2019).
- Chandra, S., Girvan, M. & Ott, E. Complexity reduction ansatz for systems of interacting orientable agents: beyond the Kuramoto model. *Chaos* **29**, 053107 (2019).
- Chandra, S. & Ott, E. Observing microscopic transitions from macroscopic bursts: Instability-mediated resetting in the incoherent regime of the d -dimensional generalized Kuramoto model. *Chaos* **29**, 033124 (2019).
- Van Hemmen, J. & Wreszinski, W. Lyapunov function for the Kuramoto model of nonlinearly coupled oscillators. *J. Stat. Phys.* **72**, 145–166 (1993).
- Mirrollo, R. & Strogatz, S. The spectrum of the locked state for the Kuramoto model of coupled oscillators. *Phys. D* **205**, 249–266 (2005).
- Markdahl, J., Thunberg, J. & Gonçalves, J. High-dimensional Kuramoto models on Stiefel manifolds synchronize complex networks almost globally. *Automatica* **113**, 108736 (2020).
- Markdahl, J. Synchronization on Riemannian manifolds: multiply connected implies multistable. *IEEE Trans. Autom. Control* (2021).
- Zhu, J. High-dimensional Kuramoto model limited on smooth curved surfaces. *Phys. Lett. A* **378**, 1269–1280 (2014).
- Thunberg, J., Markdahl, J., Bernard, F. & Gonçalves, J. Lifting method for analyzing distributed synchronization on the unit sphere. *Automatica* **96**, 253–258 (2018).
- Lageman, C. & Sun, Z. Consensus on spheres: convergence analysis and perturbation theory. In *Proc. 55th Conference on Decision and Control (CDC)*. 19–24 (2016).
- Schwerdtfeger, P., Wirz, L. N. & Avery, J. The topology of fullerenes. *WIRES Comput. Mol. Sci.* **5**, 96–145 (2015).
- Hinrichsen, D. & Pritchard, A. J. *Mathematical Systems Theory I: Modelling, State Space Analysis, Stability and Robustness*. Vol. 48 (Springer, 2011).
- Dai, X. et al. Discontinuous transitions and rhythmic states in the D -dimensional Kuramoto model induced by a positive feedback with the global order parameter. *Phys. Rev. Lett.* **125**, 194101 (2020).
- Ha, S.-Y., Kang, M. & Kim, D. Emergent behaviors of high-dimensional Kuramoto models on Stiefel manifolds. <https://arxiv.org/abs/2101.04300> (2021).
- James, I. M. *The Topology of Stiefel Manifolds*. Vol. 24 (Cambridge University Press, 1976).
- Zhang, J., Zhu, J. & Qian, C. On equilibria and consensus of the Lohe model with identical oscillators. *SIAM J. Appl. Dyn. Syst.* **17**, 1716–1741 (2018).
- Kahan, W. Spectra of nearly hermitian matrices. *Proc. Am. Math. Soc.* **48**, 11–17 (1975).
- Chikuse, Y. *Statistics on Special Manifolds*. Vol. 174 (Springer Science and Business Media, 2012).

Acknowledgements

J.M. is supported by the University of Luxembourg IRP OptBioSys. D.P., L.M., and J.G. acknowledge support from the FNR through CORE OPEN SYBION, ref. O19/13904037. D.P. is supported by the FNR PRIDE DTU CtiTiCS, ref. 10907093. J.G. is partly supported by the 111 Project on Computational Intelligence and Intelligent Control, ref. B18024.

Author contributions

J.M., D.P., and J.G. designed the study. J.M., D.P., and L.M. developed the model. J.M. implemented the model. J.M., D.P., and L.M. analyzed and interpreted the results. J.G. supervised and coordinated the project. J.M. and D.P. wrote the first draft. All authors contributed to the final draft. All authors gave their final approval for publication.

Competing interests

The authors declare no competing interests.

Additional information

Supplementary information The online version contains supplementary material available at <https://doi.org/10.1038/s42005-021-00689-y>.

Correspondence and requests for materials should be addressed to J.M.

Peer review information *Communications Physics* thanks the anonymous reviewers for their contribution to the peer review of this work. Peer reviewer reports are available.

Reprints and permission information is available at <http://www.nature.com/reprints>

Publisher's note Springer Nature remains neutral with regard to jurisdictional claims in published maps and institutional affiliations.



Open Access This article is licensed under a Creative Commons Attribution 4.0 International License, which permits use, sharing, adaptation, distribution and reproduction in any medium or format, as long as you give appropriate credit to the original author(s) and the source, provide a link to the Creative Commons license, and indicate if changes were made. The images or other third party material in this article are included in the article's Creative Commons license, unless indicated otherwise in a credit line to the material. If material is not included in the article's Creative Commons license and your intended use is not permitted by statutory regulation or exceeds the permitted use, you will need to obtain permission directly from the copyright holder. To view a copy of this license, visit <http://creativecommons.org/licenses/by/4.0/>.

© The Author(s) 2021